



Original Article

Potential SARS-CoV-2 Nonstructural Protein 15 Inhibitors: Repurposing FDA-approved Drugs

Jason Y Tang¹, Igor F. Tsigelny^{1,2,3*} , Jerry P. Greenberg¹, Mark A. Miller¹ and Valentina L. Kouznetsova^{1,3}

¹San Diego Supercomputer Center, University of California, San Diego, California, USA; ²Department of Neurosciences, University of California, San Diego, California, USA; ³BiAna, California, USA

Received: August 23, 2021 | Revised: September 18, 2021 | Accepted: September 22, 2021 | Published: October 14, 2021

Abstract

Background and objectives: Severe acute respiratory syndrome coronavirus (SARS-CoV) 2 infection has caused millions of deaths worldwide, pushing the urgent need for an efficient treatment. Nonstructural protein 15 (NSP15) is a promising target due to its importance for SARS-CoV-2's evasion of the host's innate immune response.

Methods: Using the crystal structure of SARS-CoV-2 NSP15 endoribonuclease, we developed a pharmacophore model of the functional centers in the NSP15 inhibitor's binding pocket. With this model, we conducted data mining of the conformational database of FDA-approved drugs. The conformations of these compounds underwent three-dimensional fingerprint similarity clustering, and possible conformers were docked to the NSP15 binding pocket. We also simulated the docking of random compounds to the NSP15 binding pocket for comparison.

Results: This search identified 170 compounds as potential inhibitors of SARS-CoV-2 NSP15. The mean free energy of docking for the group of potential inhibitors was significantly less than that for the group of random compounds. Twenty-one of the compounds identified as potential NSP15 inhibitors were antiviral compounds that inhibited a range of viruses, including Middle East respiratory syndrome, SARS-CoV, and even SARS-CoV-2. Eight of the selected antiviral compounds in cluster A are pyrimidine analogues, six of which are currently used in a clinical setting. Four tyrosine kinase inhibitors were identified with potential SARS-CoV-2 inhibition, which is consistent with previous studies showing some kinase inhibitors acting as antiviral drugs.

Conclusions: We recommend that the 21 selected antiviral compounds are tested as COVID-19 therapeutics.

Keywords: SARS-CoV-2; Nonstructural protein 15; NSP15; FDA-approved drugs; Pharmacophore; Drug repurposing; RNA uridylyte-specific endoribonuclease; Poly(U)-specific endoribonuclease.

Abbreviations: 5'-UMP, uridine-5'-monophosphate; COVID-19, coronavirus disease 2019; HCV, hepatitis C virus; HIV, human immunodeficiency virus; MD, molecular dynamics; NSP15, nonstructural protein 15; ORF, open reading frame; PDB, protein data bank; SARS-CoV, severe acute respiratory syndrome coronavirus; VMD, visual molecular dynamics.

***Correspondence to:** Igor F. Tsigelny, San Diego Supercomputer Center, University of California, San Diego, California 92093-0505, USA; Department of Neurosciences, University of California, San Diego, California 92093-0505, USA; BiAna, California 92093-0505, USA. ORCID: <https://orcid.org/0000-0002-7155-8947>. Tel: +1-857-822-0953, Fax: +1-858-581-9073, E-mail: itsigel@ucsd.edu

How to cite this article: Tang JY, Tsigelny IF, Greenberg JP, Miller MA, Kouznetsova VL. Potential SARS-CoV-2 Nonstructural Protein 15 Inhibitors: Repurposing FDA-approved Drugs. *J Explor Res Pharmacol* 2021;6(4):137–147. doi: 10.14218/JERP.2021.00032.

Introduction

Coronavirus disease-2019 (COVID-19) is a respiratory disease caused by severe acute respiratory syndrome coronavirus (SARS-CoV) 2 infection. As of 1 August 2021, SARS-CoV-2 has cumulatively infected over 198 million people and killed over 4 million individuals in almost 200 countries and regions (www.coronavirus.jhu.edu). The serious threats to global public health and the economy presented by SARS-CoV-2 have created an urgent need to identify novel tools to provide new pharmacologic leads that can improve survival for those already infected.

SARS-CoV-2 is a positive-sense, single-stranded, RNA beta-coronavirus with a genome size of approximately 30 kb. The

genomic RNA contains a 5'-cap structure and a 3'-poly(A) tail. During infection, the viral genome is translated to generate viral polyproteins and transcribed to generate negative-sense RNA and subgenomic RNAs. The SARS-CoV-2 genome contains 14 open reading frames (ORFs) that encode 29 proteins, including non-structural proteins (NSPs), structural proteins, and accessory proteins. The two main units, ORF1a and ORF1b, are located at the 5'-terminus and produce 16 NSPs through proteolytic cleavage by two viral proteases: the 3C-like protease and the papain-like protease. NSPs are essential for RNA transcription, replication, translation, and suppression of the host antiviral response.¹⁻³

Targeting viral proteins to disrupt replication is an important approach to develop a therapy against SARS-CoV-2 infection. Ideally, one can target highly conserved viral proteins that are unlikely to acquire the resistance of new viral mutants as the outbreak progresses. Recent studies have reported SARS-CoV-2 genomic variations in over 10% of isolated sequences, with the most frequent mutations being P323L in NSP12 and D641G in the spike protein.^{4,5} In contrast, NSP15, an RNA uridylylate-specific endoribonuclease (with a C-terminal region homologous to poly(U)-specific endoribonuclease enzymes), is highly conserved, making it an attractive target for drug development. NSP15-like endoribonucleases are found in all coronavirus family members, suggesting its endonuclease function is critical for the viral life cycle. The amino-acid sequence alignment of NSP15 from SARS-CoV and SARS-CoV-2 shows 88% sequence identity and 95% sequence similarity.⁶ NSP15 recognizes uracil and cleaves single-stranded RNA through an ion of Mn^{2+} , requiring a transesterification reaction.⁷ Recent studies indicate that NSP15 is not required for viral RNA synthesis; rather, NSP15 suppresses the host protective immune response through evasion of host dsRNA sensors.⁸ Most recently, NSP15 has been reported to participate in viral RNA processing by degrading viral polyuridine sequences. This may prevent the host immune sensing system from detecting viral RNA via cell pathogen-recognition receptors, which subsequently inhibits both direct and indirect antiviral effects.⁹ These mechanisms are important for normal coronavirus infection of host cells. In the absence of NSP15 activity, viral replication is slowed significantly; therefore, NSP15 remains an attractive target for addressing SARS-CoV-2 infection.¹⁰

NSP15 is only active as a hexamer, which is formed as a dimer of trimers. The NSP15 monomer contains three domains: a N-terminal domain responsible for oligomerization, a middle domain, and a C-terminal domain, which contains the catalytic domain.¹¹ The binding sites of each of the catalytic domains are accessible despite hexamerization. A recent publication reveals the first two crystal structures of SARS-CoV-2 NSP15 with 1.90 Å and 2.20 Å resolution.⁶ In the C-terminal catalytic domain of SARS-CoV-2 NSP15, the active site carries six key residues: His235, His250, Lys290, Thr341, Tyr343, and Ser294. Among these residues, His235, His250, and Lys290 are suggested to constitute the catalytic triad for its nuclease activity. His250 acts as a general base to activate the 2'-OH of the ribose, while His235 functions as a general acid to donate a proton to the leaving 5'-OH of the ribose.^{6,11} Ser294 together with Tyr343 determine uridine specificity. Ser294 is a key residue that recognizes uracil and is assumed to interact with the carbonyl oxygen atom of uracil, while Tyr343 orients the ribose of uridine for cleavage by van der Waals interactions.¹¹ In the crystal structure of the NSP15 citrate-bound form, the citrate ion forms hydrogen bonds with active site residues including His235, His250, Lys290, and Thr341.⁶ In the crystal structure of NSP15 complexed with uridine-5'-monophosphate (5'-UMP), 5'-UMP interacts with all six active site residues. The uridine base of 5'-UMP interacts with Tyr343 through van der Waals interactions and forms hydrogen bonds with the nitrogen atom of Ser294,

Lys290, and His250.¹² This structural information is important for exploring the binding of uridine analogues as potential SARS-CoV-2 NSP15 inhibitors.

Tipiracil, a uracil derivative, is a thymidine phosphorylase inhibitor. It is an FDA-approved drug used with trifluridine to treat metastatic colorectal and gastric cancer. Previously, tipiracil has been reported to form hydrogen bonds with the SARS-CoV-2 NSP15 active site residues Ser 294, Lys345, and His250.¹² Tipiracil suppresses the RNA nuclease activity of NSP15 and modestly inhibits SARS-CoV-2 virus replication *in vitro* without affecting the viability of host cells, most likely through competitive inhibition.¹² Moreover, recent *in-silico*-based approaches have identified other potential NSP15 inhibitors that await further structural and biochemical validation.^{13,14} The current COVID-19 pandemic has brought attention to the repurposing of existing drugs and the rapid identification of candidate compounds. In this study, we use structure-based pharmacophore modeling and molecular docking to identify potential inhibitors of NSP15 by screening the FDA-approved drug database.

Methods

The crystal structure of SARS-CoV-2 NSP15 endoribonuclease (protein data bank (PDB) ID: 6WXC) complexed with the ligand tipiracil (5-chloro-6-(1-(2-iminopyrrolidinyl)methyl)uracil) was downloaded from the RCSB protein data bank. Using Molecular Operating Environment (MOE; CCG, Montreal, Canada), we analyzed the key binding site residues that are responsible for the interaction between NSP15 and tipiracil and employed a structure-based approach to construct our pharmacophore model of NSP15. The default forcefield used was Amber 10: EHT with R Field solvation. Our pharmacophore model was created with seven features and excluded volume $R = 1.6$ Å. It had one donor, three acceptors, one cationic atom and donor, and two hydrophobic centroids. Based on this developed pharmacophore, we conducted a pharmacophore search on our conformational database of 2,356 FDA-approved drugs. A pharmacophore partial match was used for a 5-of-7 features search.

For multi-conformational docking of the selected compounds, we prepared the NSP15 structure with the Protonate 3D application, isolated the ligand and pocket, visualized the space available for the docked ligands, defined the binding pocket based on the known key residues for its nuclease activity and uridine specificity, and generated ligand conformations using the bond rotation method. The compounds were docked into the pocket using the Triangle Matcher Method and London dG scoring for placement as well as the Induced Fit Method and GBVI/WSA dG scoring for refinement. Poses were ranked by the GBVI/WSA binding free energy calculation in the S field. The 56 random control compounds were selected from the FDA drug database.

To further analyze the ligand interactions for some of the above models, the structures were divided into ligand and protein pdb files. The separate structures were protonated: the protein with Visual Molecular Dynamics (VMD), v1.9.4, and the ligand with Avogadro, v1.2.0. VMD was used to generate a psf (NAMD protein structure file) file for the protein, and the Ligand Reader and Modeler from charmm-gui.org was used to generate the psf and prm files for the ligand. VMD was then used with the CHARMM36 forcefield to recombine the ligand and protein, thus solvating the structure and generating the required psf and pdb files.¹⁵⁻¹⁷ NAMD v2.14 was used to run 100 steps of minimization followed by 100 ns of dynamics with 2 fs/step (50,000,000 iterations). The simulation

conditions were rigid bonds involving hydrogen (rigid bonds set to “all”), a splitting distance of 12 Å between the short-range and the particle-mesh Ewald long-range potential, Langevin dynamics at 310K with hydrogen atoms excluded (Langevin hydrogen set to “off”), and periodic boundary conditions.^{15–17} The MD simulations were run on the San Diego Supercomputer Center Expanse Cluster (https://www.sdsc.edu/support/user_guides/expanse.html) on 2 nodes, 128 cores per node for a total of 256 processors.

Results

Pharmacophore model creation and search of drug database

A recent publication of the crystal structure of the SARS-CoV-2 NSP15 endoribonuclease complexed with the ligand tipiracil provides detailed information regarding key residues responsible for the catalytic activity of NSP15 and its interactions with potential ligands.⁶ Based on the binding information for these key residues, we generated a pharmacophore model with potential functional centers that bind to the residues in the pocket (Fig. 1a).

The pharmacophore search with a partial match of 5 of 7 centers identified 803 compounds. We selected 170 compounds from the search based on the numbers of hydrogen bonds and hydrophobic interactions in the best docking pose. A minimum of three hydrogen bonds and two hydrophobic interactions were the criteria for selection. We clustered the selected compounds using the Similarity Clustering of the MOE Database Viewer with a fingerprint of GpiDAPH3 and similarity-overlap parameter $SO = 45\%$. The search identified three major hit clusters containing ten or more compounds, along with several clusters containing less than ten compounds (from nine to two) and 36 single clusters with just one compound (Table 1). The two largest clusters (A and B) contain 16 and 35 compounds, respectively; clusters C, D, E, F, G, and H contain 11, 9, 7, 7, 5, and 5 compounds, respectively; clusters I, J, and K contain 4 compounds each; clusters L to V contain 2–3 compounds each; and 36 single compounds were not a part of a cluster (Table 1). Flexible alignment of the clusters was used to illustrate common features of the compounds (Figs. 1, 2). Cluster A mainly contains pyrimidine analogues that are known viral inhibitors. Cluster B mainly contains cephalosporin antibiotics. Cluster C mainly contains diuretic medications. Cluster D mainly contains angiotensin-converting enzyme inhibitors and carbapenem antibiotics. Cluster E mainly contains beta blockers. Cluster F mainly contains nonsteroidal anti-inflammatory drugs. Cluster G mainly contains tyrosine kinase inhibitors. Cluster H mainly contains fluoroquinolones. Cluster I mainly contain diuretics. Cluster J mainly contains saccharide-like compounds. Cluster K mainly contains prostaglandin-like compounds.

Computational docking

For docking the selected compounds, we used the crystal structure of SARS-CoV-2 NSP15 endoribonuclease (PDB ID: 6WXC), which was imported into MOE. After structure preparation and the model's binding pocket was defined, based on known key residues for its nuclease activity and uridine specificity, ligand conformations were generated using the bond rotation method. These were docked into the site with the Triangle Matcher method and ranked with the London dG scoring function. The retain option specifies the number of poses (30) to pass to the refinement, which is for energy minimization in the pocket, before rescoring with the Induced Fit method and

the GBVI/WSA dG scoring function. To validate docking, 56 random control compounds were selected from the FDA drug database, using a random number generator without repetitions.

The values of docking free energies of the selected and random compounds are shown in Figure 3. The means of the selected and random compounds are -6.50 kcal/mol and -5.79 kcal/mol, respectively. Furthermore, the p value of the one-tailed test for selected vs. random compounds is 1.31×10^{-6} . The energies of interaction with the NSP15 active site are shown in Table 2 and Table S1.

Molecular dynamics (MD) simulations

We selected the three compounds with the top docking energies to further analyze the stability of the ligand interactions; these compounds were cefmenoxime, cefotiam, and ceforanide. The final configurations of the compound-protein complexes resulting from these MD simulations are shown in Figure 4 and Table 3.

Cefmenoxime (Fig. 4a, d) had six major ligand interactions with NSP15, the shortest distance of which was 2.73 Å from the residue Lys290. Cefotiam (Fig. 4b, e) had four major ligand interactions with NSP15, the shortest distance of which was 2.69 Å from the residue Leu246. Finally, ceforanide (Fig. 4c, f) had two major ligand interactions with NSP15, the shortest distance of which was 2.70 Å from the residue Lys290. Figure 5 shows the measurements between the NZ atom of Lys290 of the protein and the geometric center of these compounds. Of note, these distances were fairly stable during the MD simulations.

Discussion

Based on the crystal structure of the SARS-CoV-2 NSP15 endoribonuclease complexed with tipiracil, we developed a pharmacophore model of NSP15's binding pocket, including key residues for its nuclease activity and uridine specificity. Using this model, we conducted a pharmacophore search of our conformational database of FDA-approved drugs. In the search, 170 compounds were selected, clustered, and were then used for flexible docking into the NSP15 active site pocket in the catalytic domain. Twenty-one of the compounds identified as potential NSP15 inhibitors were antiviral compounds used against a range of viruses, including human immunodeficiency virus (HIV), hepatitis C virus (HCV), hepatitis B virus, influenza, and herpes simplex virus. Some of them also demonstrated inhibitory activity against Middle East respiratory syndrome, SARS-CoV, and SARS-CoV-2 (Table 4).

According to the DrugVirus.info database,¹⁸ 13 of the antiviral compounds selected by the pharmacophore-based search displayed activity against a total of 40 viruses in cell-culture, animal, and clinical models (Fig. 6). The other eight antiviral compounds were not in the database. A previous study did not identify any of these compounds as potential NSP15 inhibitors, and their top selected drugs did not show antiviral activity.¹⁴ Differences in methodology may explain these discrepancies in the results. Specifically, Chandra and co-authors used the NSP15 (PDB ID: 6W01) structure with a citrate ion;¹⁴ we used the crystal structure of NSP15 complexed with tipiracil that binds to the NSP15 uracil site. We assume that the pharmacophore model generated with this protein structure includes the key features responsible for ligand interaction with residues in the NSP15 active site. We did notice that tipiracil, the positive control, did not have a low free energy. However, an *in-vitro* study confirmed that tipiracil can inhibit uracil binding to the NSP15 active site, presumably through com-

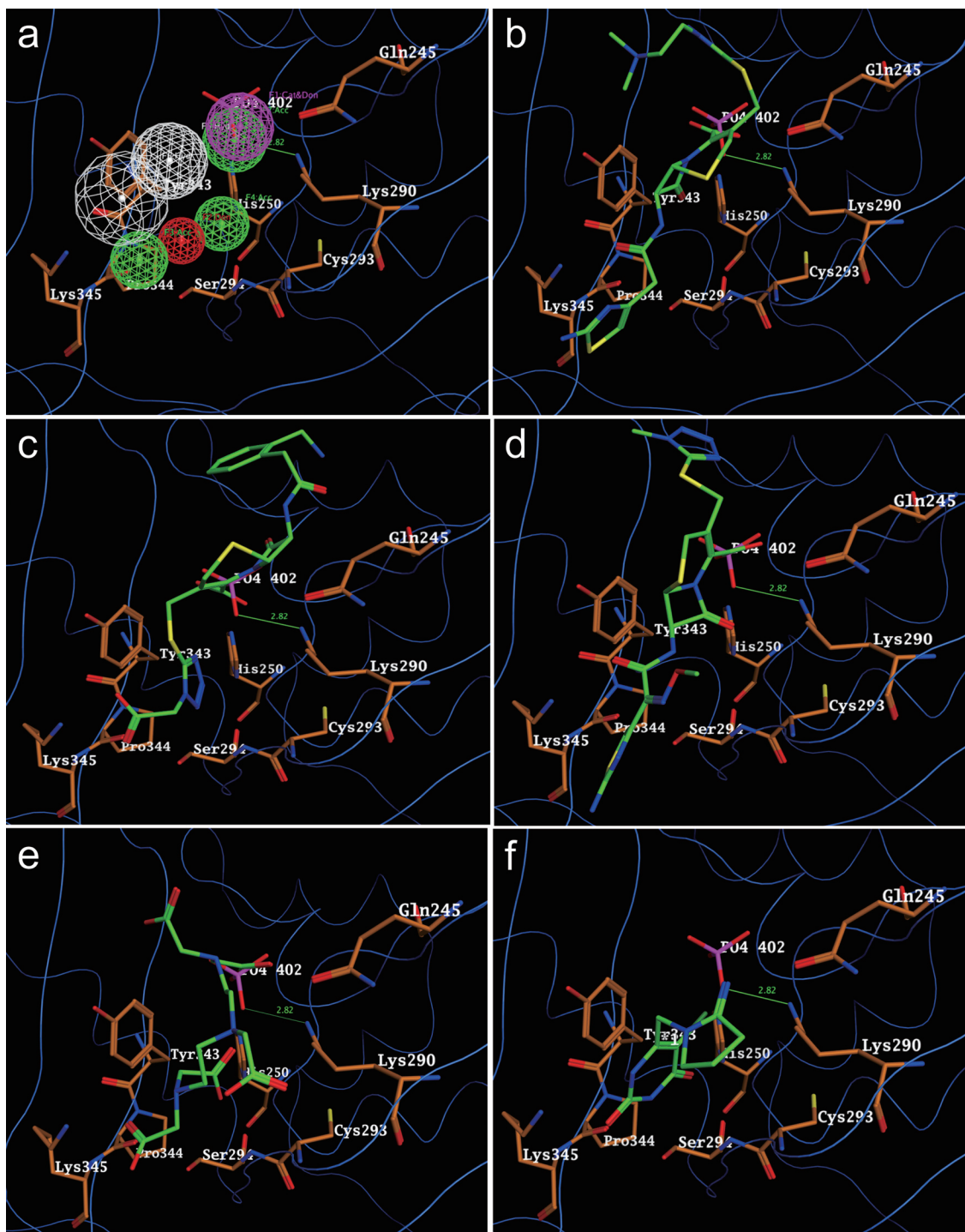


Fig. 1. Pharmacophore of the NSP15 binding pocket and binding poses of the best energy-docked molecules. (a) The model of the pharmacophore contains seven functional centers: one donor, three acceptors, one cationic atom and donor, and two hydrophobic centroids. Binding poses of the drugs with the best scores: (b) Cefotiam, DFE = -8.48 kcal/mol; (c) Ceforanide, DFE = -8.43 kcal/mol; (d) Cefmenoxime, DFE = -8.25 kcal/mol; (e) Pentetic acid, DFE = -8.20 kcal/mol. (f) Positive control, Tipiracil, DFE = -5.14 kcal/mol. DFE, Docking free energy; NSP15, nonstructural protein 15.

petitive inhibition and modestly suppressing SARS-CoV-2 viral replication in cellular assays.¹² Cluster A includes six pyrimidine analogues that are currently used as viral inhibitors: HIV reverse transcriptase inhibitors—zidovudine and stavudine, a hepatitis B

virus DNA polymerase inhibitor—telbivudine, and herpes simplex virus DNA polymerase inhibitors—brivudine, edoxudine, and trifluridine (Table 4 and Fig. 6). The other two drugs in cluster A, tipiracil¹² and floxuridine,¹⁹ are anticancer drugs that have anti-

Table 1. Drug candidates clustered by fingerprint similarity

A	Cluster					Single Drug
	B	C	F	K	S	
Aminogluthethimide	Amoxicillin	Bendroflumethiazide	Azathioprine	Alprostadil	Cimetidine	Almotriptan
Biotin	Ampicillin	Benzthiazide	Dantrolene	Dinoprostone	Famotidine	Amlodipine
Brivudine	Azlocillin	Chlorothiazide	Lornoxicam	Hydrocortamate		Amprenavir
Butabarbital	Betiatile	Cyclopentthiazide	Meloxicam	Losartan	T	Atorvastatin
Butalbital	Cefaclor	Furosemide	Nitazoxanide		Sulfadoxine	Cabergoline
Edoxudine	Cefadroxil	Hydrochlorothiazide	Nitrofurantoin	L	Sulfametopyrazine	Capecitabine
Ethosuximide	Cefamandole	Methyclothiazide	Tenoxicam	Labetalol		Citric acid
Floxuridine	Cefamandole nafate	Metolazone		Pirbuterol	U	Dexrazoxane
Glutethimide	Cefapirin	Polythiazide	G	Salbutamol	Dexpanthenol	Dofetilide
Propylthiouracil	Cefazolin	Quinethazone	Afatinib		Pantothenic acid	Doravirine
Stavudine	Cefdinir	Trichlormethiazide	Dacomitinib	M		Enoximone
Telivudine	Cefditoren		Dasatinib	Bicisate	V	Entacapone
Tipiracil	Cefmenoxime	D	Gefitinib	Edetic Acid	Peramivir	Eprosartan
Trifluridine	Cefmetazole	Doripenem	Lapatinib	Pentetic Acid	Pinacidil	Famciclovir
Uracil mustard	Cefonidic	Ertapenem				Fursultiamine
Zidovudine	Ceforanide	Etacrynic acid	H	N		Indacaterol
	Cefotaxime	Imipenem	Gatifloxacin	Riboflavin		L-Citrulline
	Cefotiam	Lisdexamfetamine	Levofloxacin	Sapropterin		Macitentan
	Cefoxitin	Meropenem	Nalidixic acid			Mannitol
	Cefpirome	Perindopril	Nedocromil	O		Methocarbamol
	Cefpodoxime	Ramipril	Trovafloxacin	Carglumic acid		Milrinone
	Cefprozil	Spirapril		Glutathione		Minocycline
	Ceftibuten		I			Nialamide
	Ceftizoxime	E	Gliclazide	P		Osetamivir
	Cephaloglycin	Acebutolol	Tolazamide	Glimepiride		Oxeladin
	Cephalothin	Atenolol	Tolbutamide	Glyburide		Ranolazine
	Cloxacillin	Bisoprolol	Torasemide			Ritiometan
	Cyclacillin	Celiprolol		Q		Rutin
	Dicloxacillin	Metipranolol		Amikacin		Sofosbuvir
	Flucloxacillin	Nadolol	Acarbose	Tobramycin		Spectinomycin
	Loracarbef	Timolol	Gaxilose			Streptomycin
	Methicillin		Lactulose	R		Streptozocin
	Mezlocillin		Mannitol busulfan	Acemetacin		Sulpiride
	Nafcillin		Tolmetin			Tazobactam
	Penicillin V					Uridine triacetate
						Xanthinol

Note: The drugs benzonatate, ceforetan, and fosamprenavir were not stable in the MD simulation and thus excluded. MD, molecular dynamics.

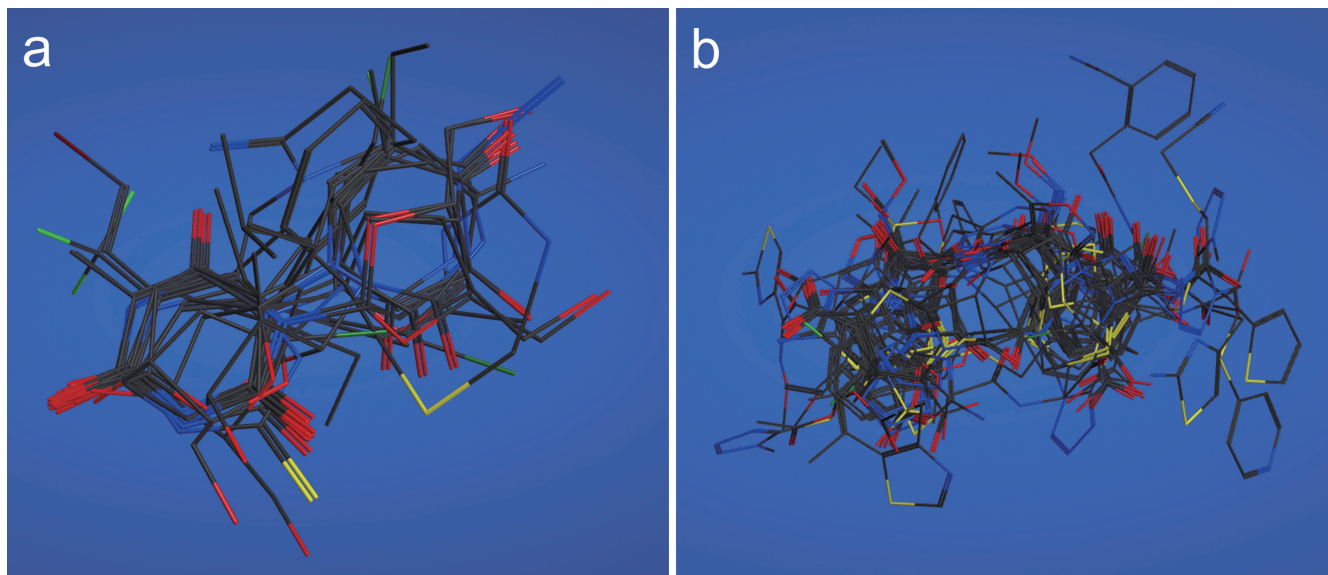


Fig. 2. Flexible alignments of compounds in clusters selected by the pharmacophore-based search of possible drug candidates in the conformational database of FDA-approved drugs. (a) Cluster A (16 compounds). (b) Cluster B (35 compounds).

ral properties. All of these pyrimidine analogues are polymerase inhibitors, which is a major class of antiviral drugs.

These results support using the pharmacophore features of

NSP15 to identify potential antiviral compounds containing a pyrimidine-like scaffold and the further development of nucleotide-like drugs with a higher affinity for the active site of NSP15.

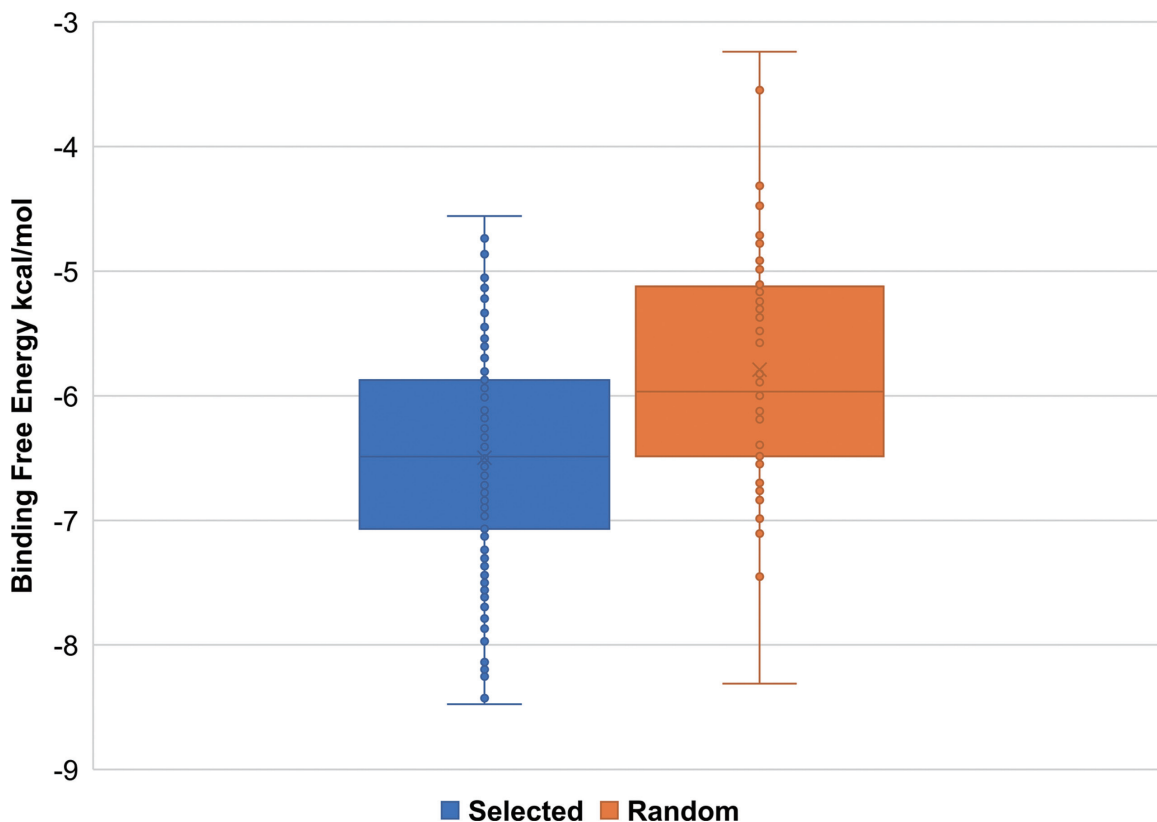


Fig. 3. Free energies of the docking interaction of selected and random compounds with SARS-CoV-2 NSP15. The means of the selected and random compounds are -6.50 and -5.79 kcal/mol, respectively. The *p* value of the one-tailed test is 1.31E-06. NSP15, nonstructural protein 15; SARS-CoV-2, severe acute respiratory syndrome coronavirus 2.

Table 2. List of selected compounds sorted by their energies of interaction with SARS-CoV-2 NSP15 in the docked positions. All compounds shown have an energy less than -7 kcal/mol

Drug Name	DFE kcal/mol	Cluster	Drug Name	DFE kcal/mol	Cluster
Cefotiam	-8.48	B	Gliclazide	-7.33	I
Ceforanide	-8.43	B	Streptomycin	-7.31	S
Cefmenoxime	-8.25	B	Amprenavir	-7.29	S
Pentetic Acid	-8.20	M	Minocycline	-7.28	S
Cefonicid	-8.14	B	Azlocillin	-7.26	B
Cephaloglycin	-7.97	B	Dasatinib	-7.26	G
Cefamandole nafate	-7.95	B	Acarbose	-7.25	J
Cefamandole	-7.94	B	Cefditoren	-7.24	B
Atorvastatin	-7.87	S	Meropenem	-7.19	D
Cefazolin	-7.79	B	Cefpirome	-7.18	B
Ertapenem	-7.70	D	Macitentan	-7.13	S
Doripenem	-7.66	D	Cefdinir	-7.12	B
Glyburide	-7.65	P	Betiatide	-7.12	B
Cefmetazole	-7.62	B	Alprostadil	-7.12	K
Dinoprostone	-7.56	K	Cefoxitin	-7.11	B
Spirapril	-7.52	D	Acemetacin	-7.11	R
Cefotaxime	-7.52	B	Ramipril	-7.09	D
Cefapirin	-7.50	B	Ranolazine	-7.07	S
Cephalothin	-7.48	B	Afatinib	-7.06	G
Ceftibuten	-7.44	B	Losartan	-7.06	K
Lapatinib	-7.42	G	Cefadroxil	-7.03	B
Cefprozil	-7.39	B	Methicillin	-7.03	B
Cefpodoxime	-7.37	B	Sofosbuvir	-7.03	S
Mezlocillin	-7.34	B			

DFE, Docking free energy; NSP15, nonstructural protein 15; SARS-CoV-2, severe acute respiratory syndrome coronavirus 2.

Recent studies have demonstrated that tyrosine kinase inhibitors have antiviral potential through inhibition of key kinases required for viral entry and replication.^{20,21} Thus, repurposing receptor tyrosine kinase inhibitors is an effective strategy in the fight against COVID-19.²² Our pharmacophore model successfully identified four tyrosine kinase inhibitors with antiviral activity in cluster G, the binding affinities of which were high. Dasatinib, an approved drug for chronic myelogenous leukemia, has activity against both Middle East respiratory syndrome-CoV and SARS-CoV *in vitro* and possible protection against SARS-CoV-2 infection.^{23,24} The epidermal growth factor receptor inhibitor gefitinib has demonstrated *in-vitro* activity against HCV, BK virus, cytomegalovirus, and vaccinia virus (Fig. 6). In addition, lapatinib was recently found to potently inhibit SARS-CoV-2 replication at clinical doses, strongly supporting our screening result.²⁵

Promising antiviral drugs from cluster U include the HIV proteinase inhibitor amprenavir. Specifically, amprenavir has a free energy of -7.29 kcal/mol and modestly inhibits replication of SARS-CoV-2 *in vitro*.²⁶ Outside of clusters A, G, and U, other antiviral drugs include the influenza neuraminidase inhibitors peramivir and oseltamivir, the HIV non-nucleoside reverse transcriptase inhibitor doravirine, and the HCV NS5B polymer-

ase inhibitor sofosbuvir, which displays activity against SARS-CoV-2.²⁷

It is interesting to note that some of the randomly selected FDA-approved drugs had free energies less than -7.00 kcal/mol, namely gadoxetate (-8.31 kcal/mol), iohexol (-7.45 kcal/mol), and chlortetracycline (-7.11 kcal/mol) (Table S1). These compounds also can be potential inhibitors of NSP15.

Future directions

We have identified potential NSP15 inhibitors through computer-based screening. These compounds will be further investigated for their effects on the endoribonuclease activity of NSP15 and the viral replication of SARS-CoV-2 using biochemical and cellular assays, respectively. Crystallization of NSP15 complexes with the potential inhibitor will also be conducted. NSP15 has been reported to be responsible for the interference with the innate immune response; thus, animal model and *in vivo* studies are needed to determine the efficacy, toxicity, and antiviral mechanism of the candidate compounds.

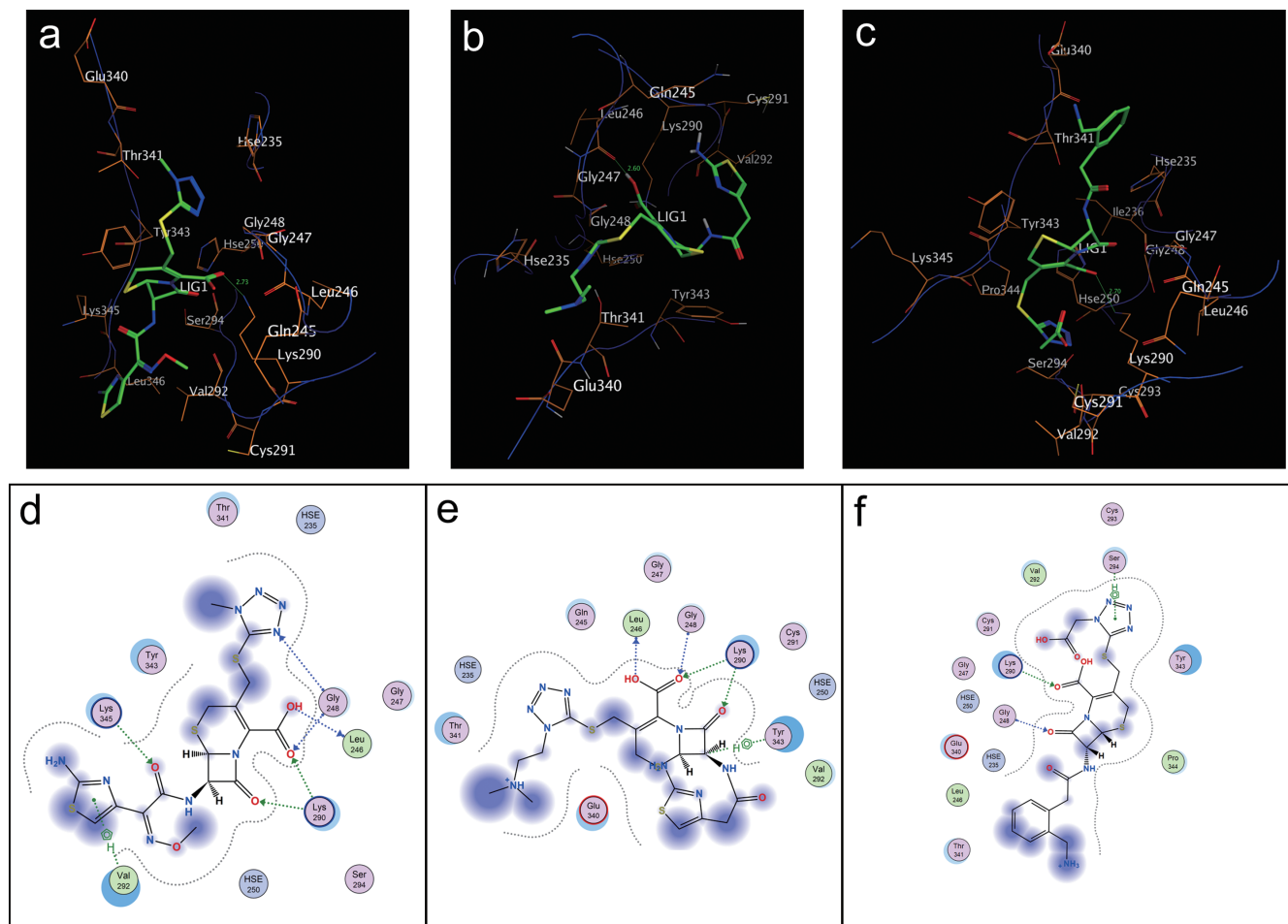


Fig. 4. Further analysis of the top three compounds in terms of the docking energies with the NSP15 binding pocket. (a, d) Cefmenoxime; (b, e) Cefotiam; (c, f) Ceforanide. NSP15, nonstructural protein 15.

Table 3. List of ligand interactions with the NSP15 binding pocket, distance, and energy for the compounds in Figure 4

	Ligand		Receptor	Interaction	Distance	Energy (kcal/mol)
<i>Cefmenoxime</i>						
	OXT	6	O	Leu246	H-donor	-5.0
	O1	7	N	Gly248	H-acceptor	-0.5
	O1	7	NZ	Lys290	H-acceptor	-6.7
	O2	10	NZ	Lys290	H-acceptor	-4.0
	O3	14	CE	Lys345	H-acceptor	-0.8
	N9	33	N	Gly248	H-acceptor	-0.6
<i>Cefotiam</i>						
	OXT	6	O	Leu246	H-donor	-2.8
	O1	7	N	Gly248	H-acceptor	-2.0
	O1	7	NZ	Lys290	H-acceptor	-3.3
	O2	10	NZ	Lys290	H-acceptor	-7.9
<i>Ceforanide</i>						
	O1	6	NZ	Lys290	H-acceptor	-4.6
	O2	10	N	Gly248	H-acceptor	-5.8

NSP15, nonstructural protein 15.

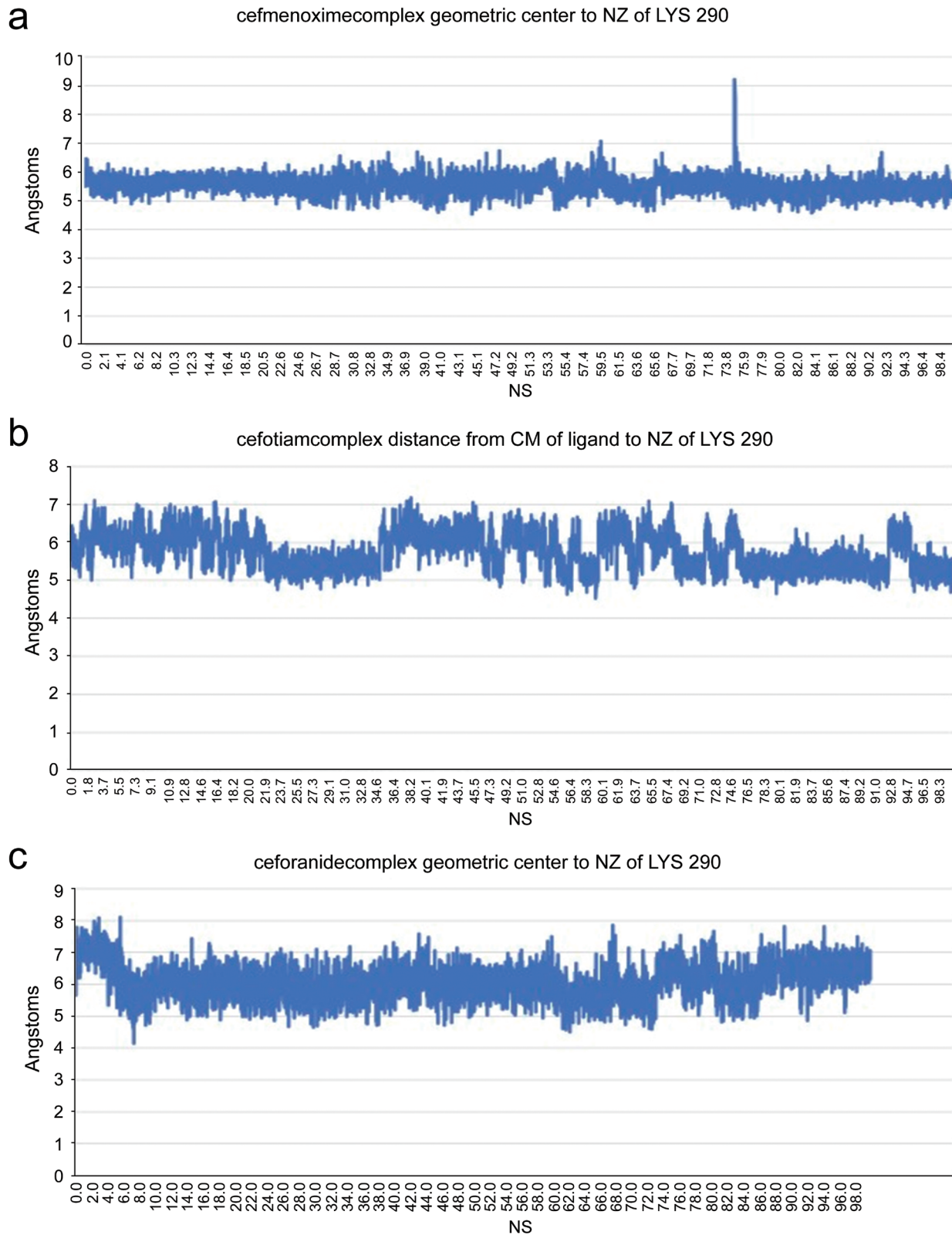


Fig. 5. Distances between the NZ atom of Lys290 of NSP15 protein and the geometric centers of the compounds during the 100 ns of MD simulation. (a) Cefmenoxime; (b) Cefotiam; (c) Ceforanide. The plots show the stability of the positions of these compounds. MD, molecular dynamics; NSP15, nonstructural protein 15.

Table 4. List of selected compounds with known antiviral activity

Cluster A	Cluster F	Cluster G	Cluster W	Cluster U	Single drugs
Trifluridine	Nitazoxanide	Gefitinib	Peramivir	Amprenavir	Oseltamivir
Zidovudine		Dasatinib			Famciclovir
Floxuridine		Lapatinib			Sofosbuvir
Stavudine		Afatinib			Doravirine
Telbivudine					Minocycline
Brivudine					
Edoxudine					
Tipiracil					

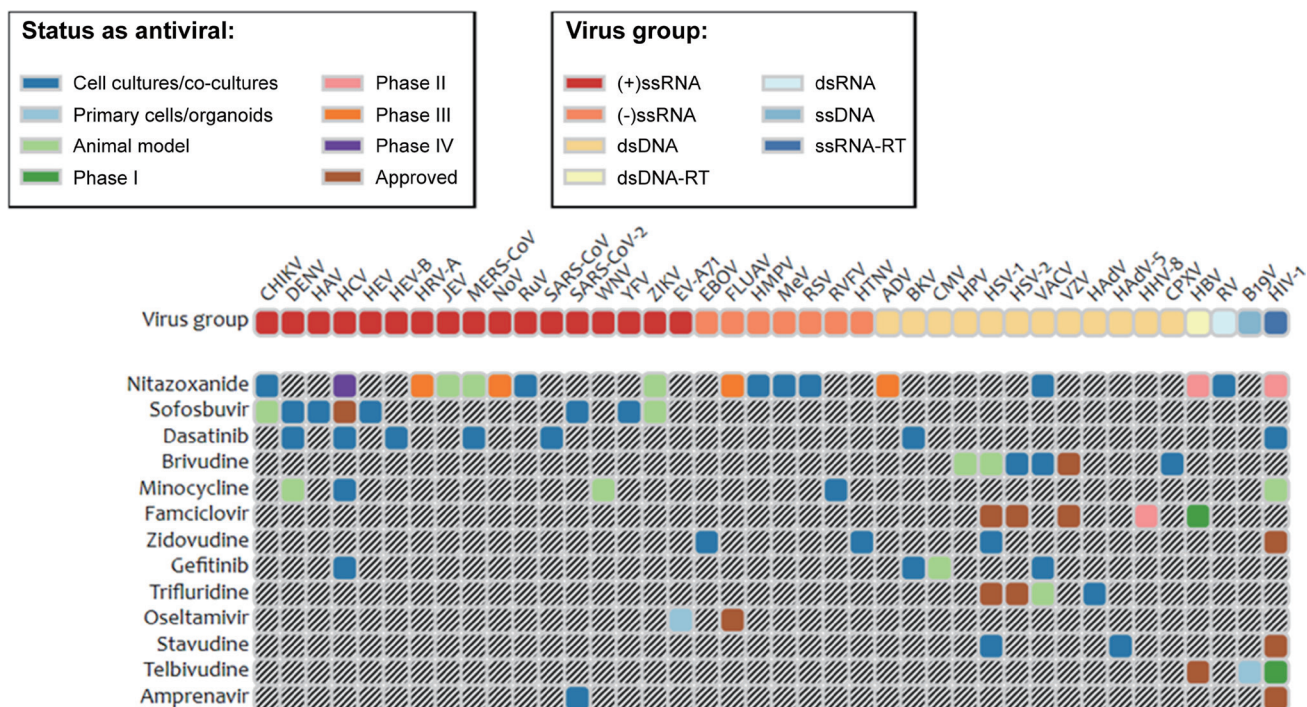


Fig. 6. A chart representing 13 of the selected antiviral drugs and their use against different viruses. Data were obtained using the DrugVirus.info database.¹⁸

Conclusions

Given the severity of the COVID-19 pandemic, we need a fast way of discovering treatments. The identification of FDA-approved drugs that inhibit SARS-CoV-2 infection can lead to advances in this field. Though this study is limited due to only using computer-based screening, the potential of the 170 compounds is a key step in finally finding a treatment. Twenty-one of these drugs have known antiviral properties, some of which have demonstrated inhibition of SARS-CoV-2 replication *in vitro*. We recommend that the 21 selected antiviral compounds are tested as COVID-19 therapeutics, especially those in clusters A, G, and U.

Supporting information

Supplementary material for this article is available at <https://doi.org/10.14218/JERP.2021.00032>.

[org/10.14218/JERP.2021.00032](https://doi.org/10.14218/JERP.2021.00032).

Table S1. List of random compounds sorted by their energies of interaction with SARS-CoV-2 NSP15 in the docked positions. DFE, docking free energy.

Acknowledgments

We would like to thank the members of the San Diego Super-computer Center and the Chemical Computing Group (Montreal, Canada).

Funding

None.

Conflict of interest

Prof. Igor F. Tsigelny is a President of BiAna, and Prof. Valentina L. Kouznetsova is the CEO of BiAna. The authors have no other conflicts of interest related to this publication.

Author contributions

JYT participated in the design of the study, performed the docking computational experiments, analyzed the data, and drafted the manuscript. IFT and VLK proposed the study concept and conducted pharmacophore development, database searching, project guidance, and manuscript writing and editing. JPG conducted molecular dynamics simulations. JPG and MAM participated in the design of the study concept as well as wrote and edited the manuscript. All authors reviewed and approved the final manuscript.

Data sharing statement

No additional data are available.

References

- Romano M, Ruggiero A, Squeglia F, Maga G, Berisio R. A structural view of SARS-CoV-2 RNA replication machinery: RNA synthesis, proofreading and final capping. *Cells* 2020;9(5):1267. doi:10.3390/cells9051267.
- Kim D, Lee JY, Yang JS, Kim JW, Kim VN, Chang H. The architecture of SARS-CoV-2 transcriptome. *Cell* 2020;181(4):914–921.e10. doi:10.1016/j.cell.2020.04.011.
- Yao H, Song Y, Chen Y, Wu N, Xu J, Sun C, *et al.* Molecular architecture of the SARS-CoV-2 virus. *Cell* 2020;183(3):730–738.e13. doi:10.1016/j.cell.2020.09.018.
- Ugurel OM, Ata O, Turgut-Balik D. An updated analysis of variations in SARS-CoV-2 genome. *Turk J Biol* 2020;44(3):157–167. doi:10.3906/biy-2005-111.
- Toyoshima Y, Nemoto K, Matsumoto S, Nakamura Y, Kiyotani K. SARS-CoV-2 genomic variations associated with mortality rate of COVID-19. *J Hum Genet* 2020;65(12):1075–1082. doi:10.1038/s10038-020-0808-9.
- Kim Y, Jedrzejczak R, Maltseva NI, Wilamowski M, Endres M, Godzik A, *et al.* Crystal structure of Nsp15 endoribonuclease NendoU from SARS-CoV-2. *Protein Sci* 2020;29(7):1596–1605. doi:10.1002/pro.3873.
- Bhardwaj K, Sun J, Holzenburg A, Guarino LA, Kao CC. RNA recognition and cleavage by the SARS coronavirus endoribonuclease. *J Mol Biol* 2006;361(2):243–256. doi:10.1016/j.jmb.2006.06.021.
- Deng X, Hackbart M, Mettelman RC, O'Brien A, Mielech AM, Yi G, *et al.* Coronavirus nonstructural protein 15 mediates evasion of dsRNA sensors and limits apoptosis in macrophages. *Proc Natl Acad Sci USA* 2017;114(21):E4251–E4260. doi:10.1073/pnas.1618310114.
- Hackbart M, Deng X, Baker SC. Coronavirus endoribonuclease targets viral polyuridine sequences to evade activating host sensors. *Proc Natl Acad Sci USA* 2020;117(14):8094–8103. doi:10.1073/pnas.1921485117.
- Ortiz-Alcantara J, Bhardwaj K, Palaninathan S, Frieman M, Baric R, Kao C. Small molecule inhibitors of the SARS-CoV Nsp15 endoribonuclease. *Virus Adapt Treat* 2010;2:125–133. doi:10.2147/VAAT.S12733.
- Pillon MC, Frazier MN, Dillard LB, Williams JG, Kocaman S, Krahn JM, *et al.* Cryo-EM structures of the SARS-CoV-2 endoribonuclease Nsp15 reveal insight into nuclease specificity and dynamics. *Nat Commun* 2021;12(1):636. doi:10.1038/s41467-020-20608-z.
- Kim Y, Wower J, Maltseva N, Chang C, Jedrzejczak R, Wilamowski M, *et al.* Tipiracil binds to uridine site and inhibits Nsp15 endoribonuclease NendoU from SARS-CoV-2. *Commun Biol* 2021;4(1):193. doi:10.1038/s42003-021-01735-9.
- Sinha SK, Shakya A, Prasad SK, Singh S, Gurav NS, Prasad RS, *et al.* An *in-silico* evaluation of different saikosaponins for their potency against SARS-CoV-2 using NSP15 and fusion spike glycoprotein as targets. *J Biomol Struct Dyn* 2021;39(9):3244–3255. doi:10.1080/07391102.2020.1762741.
- Chandra A, Gurjar V, Qamar I, Singh N. Identification of potential inhibitors of SARS-COV-2 endoribonuclease (EndoU) from FDA approved drugs: a drug repurposing approach to find therapeutics for COVID-19. *J Biomol Struct Dyn* 2021;39(12):4201–4211. doi:10.1080/07391102.2020.1775127.
- Jo S, Kim T, Iyer VG, Im W. CHARMM-GUI: a web-based graphical user interface for CHARMM. *J Comput Chem* 2008;29(11):1859–1865. doi:10.1002/jcc.20945.
- Brooks BR, Brooks CL 3rd, Mackerell AD Jr, Nilsson L, Petrella RJ, Roux B, *et al.* CHARMM: the biomolecular simulation program. *J Comput Chem* 2009;30(10):1545–1614. doi:10.1002/jcc.21287.
- Lee J, Cheng X, Swails JM, Yeom MS, Eastman PK, Lemkul JA, *et al.* CHARMM-GUI input generator for NAMD, GROMACS, AMBER, OpenMM, and CHARMM/OpenMM simulations using the CHARMM36 additive force field. *J Chem Theory Comput* 2016;12(1):405–413. doi:10.1021/acs.jctc.5b00935.
- Andersen PI, lanevski A, Lysvand H, Vitkauskienė A, Oksenyh V, Bjørås M, *et al.* Discovery and development of safe-in-man broad-spectrum antiviral agents. *Int J Infect Dis* 2020;93:268–276. doi:10.1016/j.ijid.2020.02.018.
- Petrowsky H, Roberts GD, Kooby DA, Burt BM, Bennett JJ, Delman KA, *et al.* Functional interaction between fluorodeoxyuridine-induced cellular alterations and replication of a ribonucleotide reductase-negative herpes simplex virus. *J Virol* 2001;75(15):7050–7058. doi:10.1128/JVI.75.15.7050-7058.2001.
- Schor S, Einav S. Repurposing of kinase inhibitors as broad-spectrum antiviral drugs. *DNA Cell Biol* 2018;37(2):63–69. doi:10.1089/dna.2017.4033.
- Kumar N, Sharma NR, Ly H, Parslow TG, Liang Y. Receptor tyrosine kinase inhibitors that block replication of influenza A and other viruses. *Antimicrob Agents Chemother* 2011;55(12):5553–5559. doi:10.1128/AAC.00725-11.
- Hondermarck H, Bartlett NW, Nurcombe V. The role of growth factor receptors in viral infections: an opportunity for drug repurposing against emerging viral diseases such as COVID-19? *FASEB Bioadv* 2020;2(5):296–303. doi:10.1096/fba.2020-00015.
- Dyall J, Coleman CM, Hart BJ, Venkataraman T, Holbrook MR, Kindrachuk J, *et al.* Repurposing of clinically developed drugs for treatment of Middle East respiratory syndrome coronavirus infection. *Antimicrob Agents Chemother* 2014;58(8):4885–4893. doi:10.1128/AAC.03036-14.
- Abruzzese E, Luciano L, D'Agostino F, Trawinska MM, Pane F, De Fabritiis P. SARS-CoV-2 (COVID-19) and chronic myeloid leukemia (CML): a case report and review of ABL kinase involvement in viral infection. *Mediterr J Hematol Infect Dis* 2020;12(1):e2020031. doi:10.4084/MJHID.2020.031.
- Raymonda MH, Ciesla JH, Monaghan M, Leach J, Asantewaa G, Smorodintsev-Schiller LA, *et al.* Pharmacologic profiling reveals lapatinib as a novel antiviral against SARS-CoV-2 *in vitro*. *bioRxiv* [Preprint] 2020:2020.11.25.398859. doi:10.1101/2020.11.25.398859.
- Shema Mugisha C, Vuong HR, Puray-Chavez M, Bailey AL, Fox JM, Chen RE, *et al.* A simplified quantitative real-time PCR assay for monitoring SARS-CoV-2 growth in cell culture. *mSphere* 2020;5(5):e00658–20. doi:10.1128/mSphere.00658-20.
- Jácome R, Campillo-Balderas JA, Ponce de León S, Becerra A, Lázcano A. Sofosbuvir as a potential alternative to treat the SARS-CoV-2 epidemic. *Sci Rep* 2020;10(1):9294. doi:10.1038/s41598-020-66440-9.